


# Influence of cooling atmosphere on the structure, magnetization, and dielectric properties of $CaBaCo_4O_7$

Gaoshang Gong(龚高尚), Minghao Wang(王明豪), Ruoshui Liu(刘若水), Yang Wu(吴杨), Lichen Wang(王利晨), Yongqiang Wang(王永强), and Baogen Shen(沈保根)

**Citation:**Chin. Phys. B, 2025, 34 (**4**): 047502. DOI: 10.1088/1674-1056/adbadc
Journal homepage: http://cpb.iphy.ac.cn; http://iopscience.iop.org/cpb

**What follows is a list of articles you may be interested in**

---

## Electronic structure and coexisting topological states in ferromagnetic and antiferromagnetic phases of $MnBi_2Te_4$ quantum wires

Jian Li(李健), Zhu-Cai Yin(尹柱财), Qing-Xu Li(李清旭), and Jia-Ji Zhu(朱家骥)
Chin. Phys. B, 2025, 34 (**3**): 037501. DOI: 10.1088/1674-1056/ada551

## Simulation of magnetization process and Faraday effect of magnetic bilayer films

Sheng Gao(高升), An Du(杜安), Lei Zhang(张磊), Tian-Guang Li(李天广), and Da-Cheng Ma(马大成)
Chin. Phys. B, 2024, 33 (**9**): 097505. DOI: 10.1088/1674-1056/ad5a76

## Critical behavior of quasi-two-dimensional ferromagnet $Cr_{1.04}Te_2$

Wei Niu(钮伟), Qin-Xin Song(宋沁心), Shi-Qi Chang(常世琦), Min Wang(王敏), Kui Yuan(袁奎), Jia-Cheng Gao(高嘉程), Shuo Wang(王硕), Zhen-Dong Wang(王振东), Kai-Fei Liu(刘凯斐), Ping Liu(刘萍), Yong-Bing Xu(徐永兵), Xiao-Qian Zhang(张晓倩), and Yong Pu(普勇)
Chin. Phys. B, 2024, 33 (**7**): 077506. DOI: 10.1088/1674-1056/ad4cd8

## Theoretical characterization of the temperature-dependent saturation magnetization of magnetic metallic materials

Jin-Long Wu(吴金龙), Pan Dong(董攀), Yi He(贺屹), Yan-Li Ma(马艳丽), Zi-Yuan Li(李梓源), Qin-Yuan Yao(姚沁远), Jun Qiu(邱俊), Jian-Zuo Ma(麻建坐), and Wei-Guo Li(李卫国)
Chin. Phys. B, 2024, 33 (**7**): 077502. DOI: 10.1088/1674-1056/ad39d1

## Enhanced anomalous Hall effect in kagome magnet $YbMn_6Sn_6$ with intermediate-valence ytterbium

Longfei Li(李龙飞), Shengwei Chi(迟晟玮), Wenlong Ma(马文龙), Kaizhen Guo(郭凯臻), Gang Xu(徐刚), and Shuang Jia(贾爽)
Chin. Phys. B, 2024, 33 (**5**): 057501. DOI: 10.1088/1674-1056/ad322d

---

# Influence of cooling atmosphere on the structure, magnetization, and dielectric properties of $CaBaCo_4O_7$

Gaoshang Gong(龚高尚)[1,2], Minghao Wang(王明豪)[1,2], Ruoshui Liu(刘若水)[3], Yang Wu(吴杨)[3], Lichen Wang(王利晨)[3,†], Yongqiang Wang(王永强)[1,2,‡], and Baogen Shen(沈保根)[3]

[1] *School of Electronics and Information, Zhengzhou University of Light Industry, Zhengzhou* 450000, *China*
[2] *Henan Key Laboratory of Magnetoelectronic Information Functional Materials, Zhengzhou University of Light Industry, Zhengzhou* 450000, *China*
[3] *Ningbo Institute of Materials Technology & Engineering, Chinese Academy of Sciences, Ningbo* 315201, *China*

(Received 5 February 2025; revised manuscript received 24 February 2025; accepted manuscript online 27 February 2025)

$CaBaCo_4O_7$ has been widely studied because of its distinctive structure and magnetic properties. This study examined the influence of different cooling atmospheres on the structure, magnetic properties, and dielectric behavior of $CaBaCo_4O_7$. Samples were cooled under different atmospheric conditions to assess these influences. Our findings indicate that reduced oxygen content leads to increased lattice distortion. Since oxygen atoms play a crucial role in mediating magnetic exchange, oxygen deficiency disrupts long-range magnetic order and promotes short-range antiferromagnetic interactions. Additionally, the cooling atmosphere significantly impacts grain size, thereby affecting the dielectric constant and dielectric loss. In the argon-cooled $CaBaCo_4O_7$ (Ar) sample, oxygen deficiency reduced dielectric permittivity and increased dielectric loss.

**Keywords:** $CaBaCo_4O_7$, cooling atmosphere, magnetization, dielectric

**PACS:** 75.85.+t, 77.80.–e, 77.84.–s

**DOI:** 10.1088/1674-1056/adbadc **CSTR:** 32038.14.CPB.adbadc

## 1. Introduction

The rapid development of the information industry has increased the demand for the integration and miniaturization of related devices. Recently, multiferroic materials have garnered significant attention.[1–8] One example is single-phase magnetoelectric multiferroics, where magnetic order and electric polarization coexist. The crossed coupling between them can result in a strong magnetoelectric coupling effect. Simultaneously, these materials exhibit a pronounced domino effect, where slight changes in the microstructure can greatly influence electrical and magnetic behaviors. For instance, various physical properties can be altered in response to external conditions such as temperature, pressure, electric field, and magnetic field.[9–11] Among the different single multiferroics, the $ABaM_4O_7$ family ($A$ = Y, Ca, Ln; $M$ = Fe, Co), which exhibits competing magnetic interactions, is a hot topic because of its unique transition metal sublattice topology.[12–16]

A representative compound in the $ABaM_4O_7$ family is $CaBaCo_4O_7$. It crystallizes in the non-centrosymmetric space group $Pbn2_1$.[11–13] Alternately stacked kagome (K) and triangular (T) layers of $CoO_4$ tetrahedra along the $c$-axis form the structural framework. The corner-sharing $CoO_4$ tetrahedra form a geometrically frustrated three-dimensional network. Notably, in $CaBaCo_4O_7$, the $CoO_4$ tetrahedra expand into the kagome layer, resulting in a significant orthorhombic distortion.[19–21] This particular orthogonal structure has four non-equivalent crystallographic positions for cobalt (Co) cations. Trivalent $Co_1^{3+}$ resides in the triangular lattice layer, while divalent $Co_2^{2+}$ and $Co_3^{2+}$, as well as trivalent $Co_4^{3+}$, are located in the kagome lattice layer. The charge ordering between the $Co^{2+}$ and $Co^{3+}$ cations, coupled with the large structural distortion, relieves some of the geometric frustration.[11,18,20,22–24]

The structural characteristics of $CaBaCo_4O_7$ provide the necessary conditions for the coexistence of spontaneous magnetization and ferroelectricity.[14] The kagome layer enables the formation of various magnetic structures in $CaBaCo_4O_7$. As a result, the compound displays short-range magnetic correlations. Upon cooling to the antiferromagnetic transition temperature, it undergoes an antiferromagnetic (AFM) transition at 69 K and eventually transitions to a ferrimagnetic (FIM) ground state below a critical temperature ($T_C$) of approximately 60 K.[17,18,25,26]

However, in $CaBaCo_4O_7$, the magnetoelectric coupling effect is weak due to the antiferromagnetic spin ordering, which limits the material's potential applications. To enhance the magnetoelectric coupling effect, several methods have been explored over the past few decades to increase the magnetization intensity.[17,18,24,27–29] Impurity substitution was confirmed to be an effective way to destroy the strong indirect exchange interactions between the $Co_2^{2+}$ and $Co_3^{2+}$ ions.

Despite this, no studies have yet investigated the influence

†Corresponding author. E-mail: wanglichen@nimte.ac.cn
‡Corresponding author. E-mail: wangyq@zzuli.edu.cn

© 2025 Chinese Physical Society and IOP Publishing Ltd. All rights, including for text and data mining, AI training, and similar technologies, are reserved.

of the cooling atmosphere on the magnetoelectric properties of $CaBaCo_4O_7$. To address this gap, the effects of the cooling atmosphere on the structure, magnetization, and dielectric properties were examined. Samples of $CaBaCo_4O_7$ with different oxygen contents were prepared through quenching under various conditions.[30] X-ray diffraction (XRD) results indicated no significant difference between the diffraction patterns of samples quenched in argon (Ar) and those quenched in air. A reduction in oxygen content led to a decreased exchange distance in the superexchange interaction, resulting in enhanced antiferromagnetic interaction. Additionally, changes in the preparation process notably impacted the dielectric properties of $CaBaCo_4O_7$. For the argon-cooled $CaBaCo_4O_7$ (Ar) sample, oxygen deficiency led to a decrease in dielectric permittivity and an increase in dielectric loss.

## 2. Experiment

$CaBaCo_4O_7$ was synthesized via a solid-state reaction.[31] The oxygen vacancy concentration was controlled by cooling the material in different atmospheres. Analytical reagents $CaCO_3$, $BaCO_3$, and $Co_3O_4$ were stoichiometrically weighed and mixed. The mixture was thoroughly ground to ensure homogeneity and heated to 1173 K for decarbonation. The resulting powder was then pressed into pellets and sintered at 1373 K in air for 12 h to obtain $CaBaCo_4O_7$. For $CaBaCo_4O_7$ (air) and $CaBaCo_4O_7$ (Ar), the samples were rapidly quenched in flowing air and high-purity Ar (99.9% Ar), respectively.

The phase purity and crystal structure of the samples were analyzed using a Bruker D8 ADVANCE x-ray diffraction platform ($\lambda = 1.541867$ Å). The oxygen concentration was determined by x-ray photoelectron spectroscopy (XPS, ESCALAB 250XiESCALAB). Magnetic properties were measured using a vibrating sample magnetometer (VSM) integrated into a physical property measurement system (PPMS, Quantum Design). Dielectric properties were evaluated using an inductance-capacitance-resistance (LCR) meter (Agilent 4980A).

## 3. Results and discussion

Room-temperature powder XRD (Fig. 1) was used to examine the crystal structure and phase purity of $CaBaCo_4O_7$. No additional peaks were observed in any of the samples, indicating that they crystallized in a single phase and exhibited comparable lattice parameters. Structural refinements were performed using the space group *Pbn*21. The obtained lattice parameters, along with various *R*-factors and goodness-of-fit values, are presented in Table 1. The degree of distortion ($D$) relative to an orthogonal lattice was calculated using the following equation: $D = (b/\sqrt{3} - a)/a \times 100\%$.[18,32] The data indicate only minor differences in lattice parameters among samples prepared under different conditions. Notably, the crystal cell volume of the sample synthesized in an argon atmosphere increased slightly, likely due to enhanced lattice distortion from oxygen deficiencies. The bond lengths between cobalt and oxygen ions at the center of the bipyramid are listed in Table 1. The sample cooled in argon exhibited shorter $Co_3$–O bonds and longer $Co_4$–O bonds.

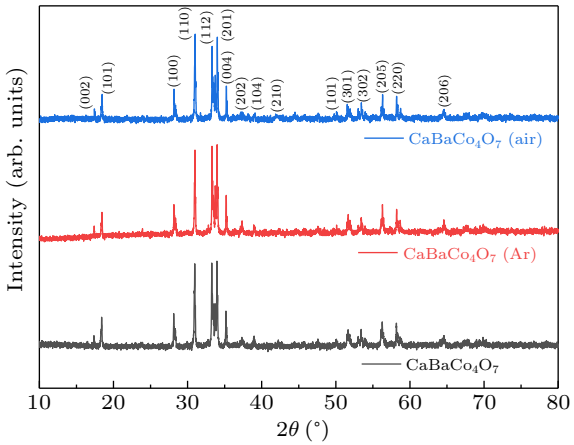



**Fig. 1.** X-ray diffraction patterns of $CaBaCo_4O_7$, $CaBaCo_4O_7$ (Ar), and $CaBaCo_4O_7$ (air).

**Table 1.** Lattice parameters, *R*-factors, goodness-of-fit values, and degree of distortion ($D$) relative to the orthogonal lattice for $CaBaCo_4O_7$, $CaBaCo_4O_7$ (Ar), and $CaBaCo_4O_7$ (air) samples.

| | Lattice parameters | | | | | | | | $R_{wp}$ | $R_p$ | $\chi^2$ | |
|---|---|---|---|---|---|---|---|---|---|---|---|---|
| | $a$ (Å) | $b$ (Å) | $c$ (Å) | $V$ (Å$^3$) | $Co_1$–O | $Co_2$–O | $Co_3$–O | $Co_4$–O | | | | $D$ |
| $CaBaCo_4O_7$ | 6.277(3) | 10.9850(5) | 10.1773(5) | 701.777(10) | 1.872(9) | 2.022(8) | 2.237(8) | 1.847(6) | 6.37% | 5.15% | 2.24 | 1.03% |
| $CaBaCo_4O_7$ (Ar) | 6.2925(3) | 11.0209(5) | 10.2019(5) | 707.512(9) | 1.874(10) | 2.065(10) | 1.790(6) | 2.013(7) | 5.68% | 3.90% | 1.70 | 1.12% |
| $CaBaCo_4O_7$ (air) | 6.2830(1) | 10.9937(3) | 10.1842(3) | 703.492(3) | 1.947(3) | 2.040(4) | 1.892(7) | 1.931(6) | 4.13% | 4.13% | 2.05 | 1.02% |

XPS measurements were performed to analyze variations in oxygen content. Figure 2(a) shows the full spectrum of the measurement results, while Figs. 2(b)–2(d) show the enlarged oxygen peaks. The oxygen content of each sample was determined by integrating the peak intensities. The results indicate a 12% reduction in oxygen content in $CaBaCo_4O_7$ (Ar) compared to $CaBaCo_4O_7$, confirming the successful introduction of oxygen vacancies.

The temperature dependence of the magnetization of the three samples measured at 0.3 T is shown in Fig. 3. The sample was cooled down to 5 K. Then, a field of $H = 3000$ Oe was applied. The zero field cooling (ZFC) magnetization curve

was measured during the warming process. The field cooling magnetization (FC) curve was measured directly during the cooling process. Both $CaBaCo_4O_7$ and $CaBaCo_4O_7$ (air) exhibited similar magnetization behavior, with magnetization intensities reaching approximately 8 emu/g at low temperatures. In contrast, the sample quenched in Ar (Fig. 3(b)) displayed lower magnetization intensity and spin-freezing temperature, indicating the critical role of oxygen in mediating magnetic exchange interactions. Higher oxygen content promotes ferrimagnetic ordering, while oxygen deficiencies suppress ferrimagnetic exchange interactions.

Figure 4 shows the temperature dependence of the inverse susceptibility for all samples, along with Curie–Weiss fitting results and Curie–Weiss temperatures ($\theta$). The negative Curie–Weiss temperature suggests a strong antiferromagnetic interaction within the samples.[33] Notably, the $\theta = -1043.5$ K for $CaBaCo_4O_7$ (Ar) confirms the enhanced antiferromagnetic exchange. This result indicates that oxygen deficiencies inhibit ferromagnetic interactions between $Co^{2+}$ and $Co^{3+}$, disrupting long-range ferromagnetic ordering and favoring short-range antiferromagnetic interactions.

Figure 5 shows the magnetization ($M$) versus magnetic field ($H$) curves of the samples measured at 5 K. The curves exhibit significant remanent magnetization and a coercive field, indicating a dominant ferrimagnetic (FIM) state. The magnetization curve of the $CaBaCo_4O_7$ sample closely overlaps with that of the $CaBaCo_4O_7$ (air) sample, which was quenched in air. The observed exchange bias in these samples can be attributed to competing ferromagnetic and antiferromagnetic exchange interactions. In contrast, the hysteresis loop of the $CaBaCo_4O_7$ (Ar) sample has a significantly smaller area, with a notably reduced exchange bias effect. This reduction is primarily due to weakened competition among various magnetic interactions.[34] Specifically, the attenuation of the exchange bias in oxygen-deficient samples may result from decreased oxygen content, which weakens interactions between magnetic ions. Consequently, the exchange bias effect is partially suppressed.

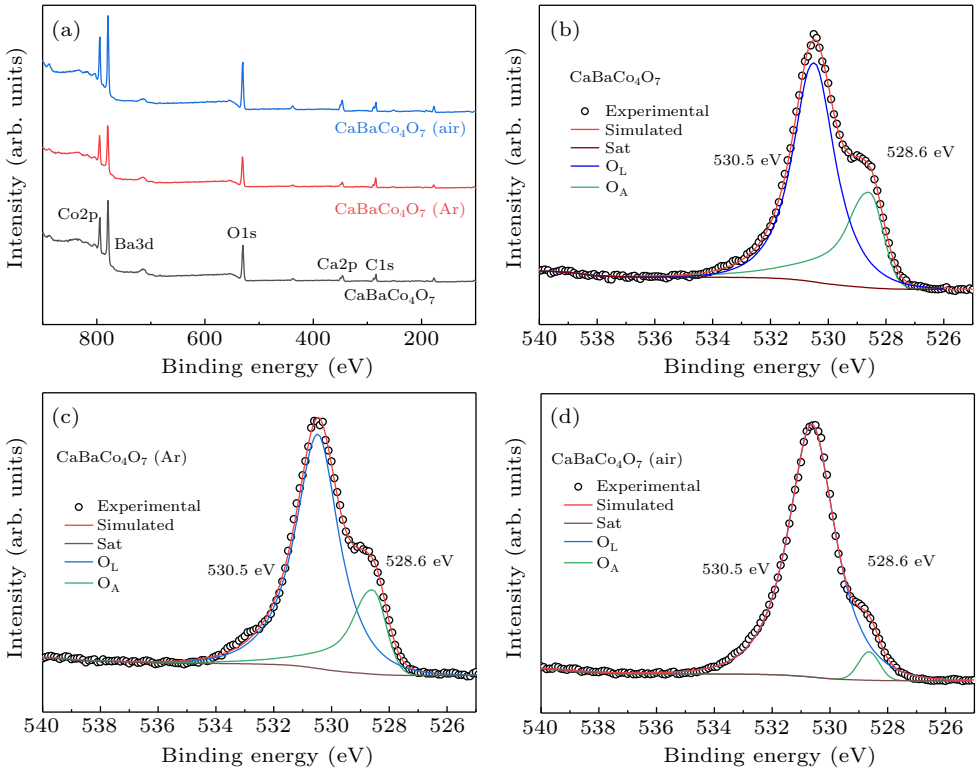



**Fig. 2.** XPS spectra of $CaBaCo_4O_7$, $CaBaCo_4O_7$ (Ar), and $CaBaCo_4O_7$ (air).

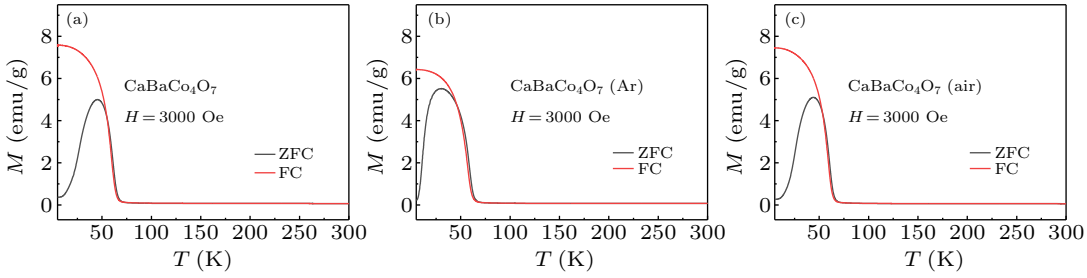



**Fig. 3.** ZFC and FC magnetization curves for (a) $CaBaCo_4O_7$, (b) $CaBaCo_4O_7$ (Ar), and (c) $CaBaCo_4O_7$ (air), the magnetic field is $H = 0.3$ T.

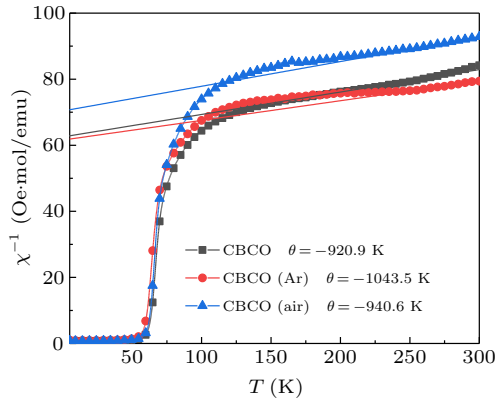



**Fig. 4.** Temperature dependence of the inverse susceptibility for (a) $CaBaCo_4O_7$, (b) $CaBaCo_4O_7$ (Ar), and (c) $CaBaCo_4O_7$ (air). The solid lines are the Curie–Weiss fitting results.

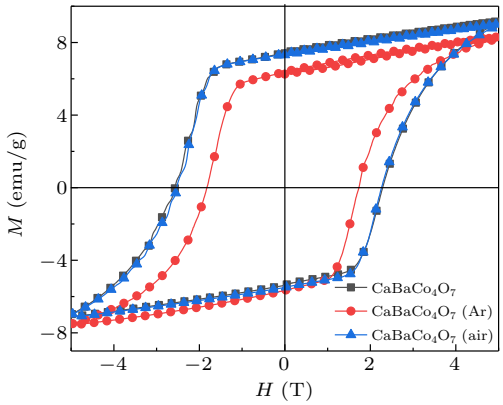



**Fig. 5.** Magnetic field dependence of magnetization for $CaBaCo_4O_7$, $CaBaCo_4O_7$ (Ar), and $CaBaCo_4O_7$ (air).

Figure 6 presents the temperature-dependent dielectric constants of the three samples measured at various frequencies ($f$ = 1 kHz, 10 kHz, 50 kHz, 100 kHz, 150 kHz, and 300 kHz). The permittivity of all samples exhibited a significant anomaly near 60 K, corresponding to the FIM transition. As seen in Figs. 3 and 5, long-range ferrimagnetic interactions are suppressed due to oxygen deficiencies. This subtle modification of the magnetic structure leads to changes in the dielectric anomaly of the $CaBaCo_4O_7$ (Ar) sample. Compared to the other two samples, the broad hump in the dielectric curve is significantly diminished in the $CaBaCo_4O_7$ (Ar) sample. Additionally, the dielectric constant of $CaBaCo_4O_7$ (air) is slightly lower than that of $CaBaCo_4O_7$. This reduction is likely due to differences in cooling rates, as cooling rate variations significantly influence grain size and the surface-to-volume ratio.[35]

Figure 7 shows the temperature-dependent dielectric loss of the samples. The dielectric loss peak exhibits a frequency shift, a characteristic feature of dielectric dispersion.[36,37] At lower temperatures, the sample prepared using the conventional method shows comparatively lower dielectric loss. However, the sample prepared in an argon atmosphere exhibits significantly higher dielectric loss. This increase can be explained by oxygen deficiency, which enhances leakage current and thereby increases dielectric loss.

It is known that the ferromagnetic component negatively contributes to the magnetodielectric effect, whereas the antiferromagnetic phase has a positive contribution. The magnetic-field-dependent magnetodielectric effect, shown in Fig. 8, indicates that the samples exhibit a dominant ferrimagnetic component at 45 K. At 70 K, dielectric permittivity increases with an increasing magnetic field, suggesting that antiferromagnetic interactions dominate at this temperature. The downward curvature of the magnetodielectric curve at high fields may result from competition between ferromagnetic and antiferromagnetic interactions. However, this curvature is absent in $CaBaCo_4O_7$ (Ar), further confirming the suppression of ferromagnetic interactions due to oxygen deficiency.

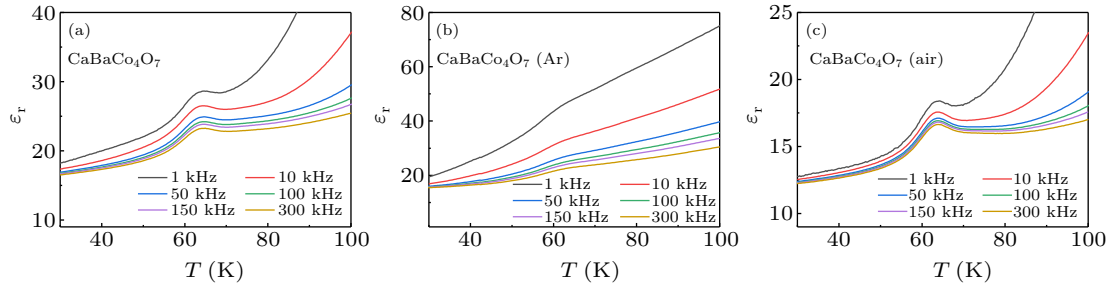



**Fig. 6.** Temperature-dependent dielectric permittivity of (a) $CaBaCo_4O_7$, (b) $CaBaCo_4O_7$ (Ar), and (c) $CaBaCo_4O_7$ (air) samples.

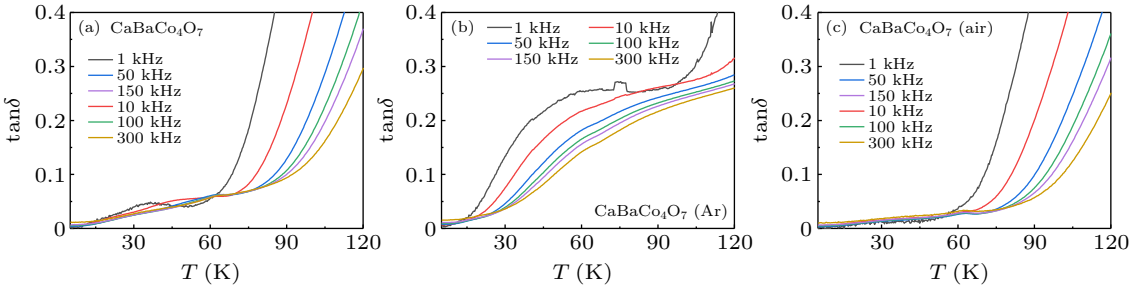



**Fig. 7.** Temperature-dependent dielectric loss for (a) $CaBaCo_4O_7$, (b) $CaBaCo_4O_7$ (Ar), and (c) $CaBaCo_4O_7$ (air) samples.

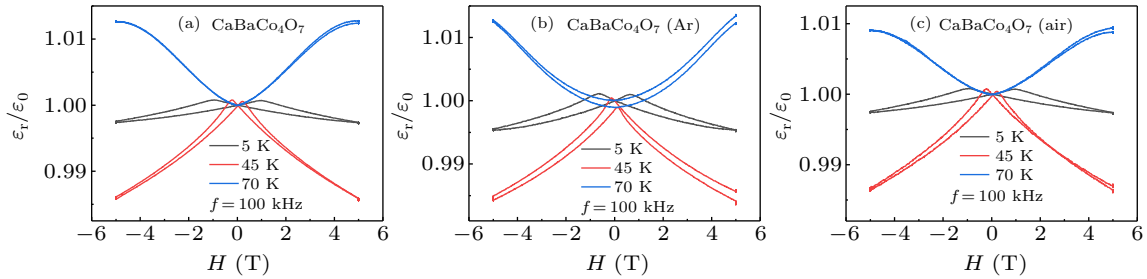



**Fig. 8.** Magnetic field dependence of the relative dielectric constant at different temperatures for (a) $CaBaCo_4O_7$, (b) $CaBaCo_4O_7$ (Ar), and (c) $CaBaCo_4O_7$ (air).

## 4. Conclusion

$CaBaCo_4O_7$ samples were prepared under different cooling atmospheres, and their structural, magnetic, dielectric, and magnetoelectric properties were investigated. The results indicate that reduced oxygen content increases orthorhombic distortion. Oxygen atoms mediate magnetic exchange interactions, and oxygen deficiency disrupts long-range magnetic order, promoting short-range antiferromagnetic interactions. The cooling atmosphere also significantly influences grain size, thereby affecting dielectric properties. For the $CaBaCo_4O_7$ (Ar) sample, a reduced dielectric permittivity was observed, attributed to oxygen deficiency. These findings provide deeper insights into the fundamental relationship between oxygen content and material properties.

## Acknowledgments

Project supported by the Key Research Project of Colleges and Universities of Henan Province (Grant No. 23A140017), the Research Project of Department of Science and Technology of Henan Province (Grant No. 242102231072), the National Natural Sciences Foundation of China (Grant No. 52402336), the special fund of the Ningbo Institute of Materials Technology and Engineering, Chinese Academy of Sciences "New magnetic materials and structural devices for 5G communication" (Grant No. E41602QB01).

## References

[1] Badr S, Saafan S A, Soliman L I, El-Nimr M K, Kamal A A, El-razek M A and El-Tahawy M 2024 *J. Magn. Magn. Mater.* **590** 171690
[2] Zhou J, Wang Y, Gong G, Duan Y, Zuo Y and Su Y 2023 *Ceram. Int.* **49** 8576
[3] Altay M, Tekşen F A, Karaaslan M and Akyol M 2024 *J. Magn. Magn. Mater.* **590** 171636
[4] Gong G, Zhou J, Wang M, Li Z, Duan Y, Zuo Y, Wang Y, Su Y and Zhang H 2023 *J. Alloys Compd.* **969** 172357
[5] Duan Y, Gong G, Wang M, Zhou J, Li Z, Zuo Y, Wang L, Wang Y, Su Y and Zhang H 2023 *Phys. B* **671** 415429
[6] Gong G, Shi C, Guo J, Zerihun G, Wang Y, Qiu Y and Su Y 2020 *J. Alloys Compd.* **820** 153099
[7] Gong G, Wang M, Chen X, He S, Man Q, Wang L, Duan Y and Li Z 2024 *Ceram. Int.* **50** 34218
[8] Gong G, Duan Y, Wang M, Li Z, Wang Y, Su Y and Qiu Y 2024 *J. Alloys Compd.* **971** 172658
[9] Cuartero V, Blasco J, Subías G, García J, Rodríguez-Velamazán J A and Ritter C 2018 *Inorg. Chem.* **57** 3360
[10] Omi T, Watanabe Y, Abe N, Sagayama H, Nakao A, Munakata K, Tokunaga Y and Arima T 2021 *Phys. Rev. B* **103** 184412
[11] Islam M, Adhikari S, Das S C, Chatterjee S, de Souza D O, Aquilanti G and Karmakar A 2023 *Mater. Res. Bull.* **161** 112173
[12] Valldor M and Andersson M 2002 *Solid State Sci.* **4** 923
[13] Tina R, He J, Wang B, Liu E and Sun Y 2023 *Chin. Phys. B* **32** 017504
[14] Raveau B, Pralong V, Caignaert V and Maignan A 2011 *Z. Anorg. Allg. Chem.* **637** 1079
[15] Caignaert V, Maignan A, Singh K, Simon C, Pralong V, Raveau B, Mitchell J F, Zheng H, Huq A and Chapon L C 2013 *Phys. Rev. B* **88** 174403
[16] Caignaert V, Pralong V, Maignan A and Raveau B 2009 *Solid State Commun.* **149** 453
[17] Wang M, Wang Y, Gong G, Li Z, Duan Y, Zuo Y, Wei M and Su Y 2024 *J. Magn. Magn. Mater.* **597** 171991
[18] Seikh M M, Sarkar T, Pralong V, Caignaert V and Raveau B 2023 *Phys. Rev. B* **86** 184403
[19] Johnson R D, Cao K and Radaelli P G 2014 *Phys. Rev. B* **90** 045129
[20] Singh K, Caignaert V, Chapon L C, Pralong V, Raveau B and Maignan A 2012 *Phys. Rev. B* **86** 024410
[21] Chai Y S, Cong J Z, He J C, Su D, Ding X X, Singleton J, Zapf V and Sun Y 2021 *Phys. Rev. B* **103** 174433
[22] Gen M, Miyake A, Yagiuchi H, Watanabe Y, Ikeda A, Matsuda Y H, Tokunaga M, Arima T and Tokunaga Y 2022 *Phys. Rev. B* **105** 214412
[23] Chatterjee S and Saha-Dasgupta T 2011 *Phys. Rev. B* **84** 085116
[24] Meher K R S P, Caignaert V, Seikh M M, Raveau B and Maignan A 2017 *Ceram. Int.* **43** 208
[25] Raoufi T, He J, Wang B, Liu E and Sun Y 2023 *Chin. Phys. B* **32** 017504
[26] Ruan C L, Yun Z Q, Hu J Y, Zhang X, Wang S G, Dai Z X, Zheng G H and Ma Y Q 2022 *J. Mater. Sci. Mater. Electron.* **33** 26881
[27] Kazei Z A, Snegirev V V, Vorob'ev G P, Popov Y F, Vyalykh D K, Kozeeva L P and Kameneva M Y 2016 *J. Exp. Theor. Phys.* **123** 1025
[28] Dhanasekhar C, Das A K and Venimadhav A 2016 *J. Magn. Magn. Mater.* **418** 76
[29] Meher K R S P, Martin C, Caignaert V, Damay F and Maignan A 2014 *Chem. Mater.* **26** 830
[30] Chandra M, Yadav S, Reen G K, Kumar A and Singh K 2019 *DAE Solid State Phys. Symp.* **2115** 030521
[31] Gong G S, Wang Y Q, Liu D W, Su Y L, Zerihun G, Qiu Y and Yuan S L 2016 *J. Mater. Sci.* **51** 73367342
[32] Oda R, Kajihara R, Nishina K, Akaki M, Kuroe H and Kuwahara H 2015 *Phys. Procedia* **75** 303
[33] Gong G S, Wang Y Q, Su Y L, Liu D W, Zerihun G and Qiu Y 2018 *Mater. Res. Bull.* **99** 419
[34] Gong G S, Guo J J, Ma Y M, Zhang Y P, Wang Y Q and Su Y L 2019 *J. Magn. Magn. Mater.* **482** 323
[35] Mao C, Dong X, Wang G, Yao C, Cao F, Cao S, Yang L and Wang Y 2009 *Acta Phys. Sin.* **58** 5784 (in Chinese)
[36] Duan Y R, Gong G S, Zuo Y Y, Zhou J, Wang L C, Wang Y Q, Su Y L and Liu D W 2023 *J. Alloys Compd.* **952** 169943
[37] Gong G S, Zhou J, Duan Y R, Hu H Y, Wang Y Q, Cheng X R and Su Y L 2022 *J. Alloys Compd.* **908** 164587